Soil Dynamics and Earthquake Engineering 155 (2022) 107167

Contents lists available at ScienceDirect

Soil Dynamics and Earthquake Engineering

journal homepage: www.elsevier.com/locate/soildyn

Field experimental investigation on broadband vibration mitigation using metamaterial-based barrier-foundation system

Benchen Zhang [a], Hsuan Wen Huang [b], Farnyuh Menq [a], Jiaji Wang [b,*], Kalyana Babu Nakshatrala [b], K.H. Stokoe [a], Y.L. Mo [b]

[a] The University of Texas at Austin, Austin, TX, USA
[b] University of Houston, Houston, TX, USA

ARTICLE INFO

Keywords:
Passive wave isolation
Periodic barrier
Periodic foundation
Hydraulic mobile shaker
Field test
Frequency response function
Vibration isolation

ABSTRACT

Both periodic barriers and periodic foundations can be used as passive isolation measures to reduce the unfavorable vibrations affecting the protected superstructure. Under a certain direction of excitation, the frequency band gaps provided by the periodic barriers and periodic foundations are usually distinguishable due to the different orientations of these subsurface structures. In this study, a series of field tests are conducted to assess the combined usage of the periodic barrier and periodic foundation in a manner to achieve better wave isolation effect. Both periodic barrier and periodic foundation used in this study are made of one-dimensional (1-D) layered periodic material. Using the state-of-art hydraulic mobile shaker (T-Rex), the excitation with various types of input signals can be applied in all the three orthogonal directions at the desired location. The arrangement of motion sensors allows for recording the response of the ground surface and the protected superstructure in all the three directions. The screening effectiveness, quantified as Frequency Response Function (FRF), of the periodic barrier and periodic foundation are discussed separately, followed by an overall evaluation of the wave isolation performance of the system composed of both periodic barrier and periodic foundation. The results show that the filtering capability of the periodic barrier and the periodic foundation is complementary to each other, and the combined usage of the periodic barrier and the periodic foundation is beneficial to mitigating the vibration of the protected superstructure.

1. Introduction

The application of periodic material in seismic isolation and man-made vibration mitigation has become an emerging technology in civil engineering. The periodic material possesses a unique frequency-selective property, meaning that the incident waves within certain frequency ranges, namely frequency band gaps, are prohibited to propagate through the periodic material. Taking advantage of this property, two types of wave isolation structures, called periodic foundation and periodic wave barrier, have been proposed and developed in recent years. A periodic foundation is the foundation constructed with the periodic material that isolates the upper structure from the ground vibrations [1–5]. A periodic wave barrier is the subsurface wave barrier composed of periodic material that blocks the incoming waves from transmitting through the barrier [6,7]. Depending on the number of directions in which the unit cells of periodic material are repeated, the periodic foundation/barrier can be further categorized into one-dimensional (1-D), two-dimensional (2-D), and three-dimensional (3-D) periodic foundation/barrier.

In the past decade, many research efforts have been made to evaluate the performance of the periodic foundation to mitigate ground vibration. Using numerical simulation, Bao et al. [8] examined the influence of various parameters (such as periodic constant, thickness ratio, number of unit cells, and angle of incident wave) on the vibration screening efficiency of 1-D periodic foundation, which provided some insights on the design of 1-D periodic foundation. Xiang et al. [9] conducted an experimental investigation on a 1-D periodic foundation using shake table tests. The tested periodic foundation was capable of reducing the peak horizontal acceleration of the superstructure by as much as 50% when the excitation frequency was within the range of frequency band gap. Zhao et al. [10] conducted both numerical simulations and experiments on a steel frame with a 1-D periodic foundation and reported that

* Corresponding author.
E-mail addresses: thebens@utexas.edu (B. Zhang), hhuang15@uh.edu (H.W. Huang), fymenq@utexas.edu (F. Menq), jwang215@central.uh.edu (J. Wang), knakshatrala@uh.edu (K.B. Nakshatrala), k.stokoe@mail.utexas.edu (K.H. Stokoe), yilungmo@central.uh.edu (Y.L. Mo).

https://doi.org/10.1016/j.soildyn.2022.107167
Received 19 August 2021; Received in revised form 16 January 2022; Accepted 18 January 2022
Available online 3 February 2022

their periodic foundation reduced the structure response by as much as 35.6% in the numerical analysis and 49% in the shaking table test. One of their findings is that the number of unit cells have slight influence on the dynamic response of the structure when the excitation frequency falls into the frequency band gap. Shi et al. [11] proposed a new configuration of 1-D periodic foundation in which discrete rubber blocks are used in lieu of the continuous rubber layer to acquire wider frequency band gaps at the lower frequency range. Based on their numerical simulations, this new configuration also provides greater level of vibration attenuation than the conventional rubber layer does. Most recently, Cheng et al. [12] carried out theoretical and numerical analyses to investigate the energy dispersion and dissipation properties of damped 1-D periodic foundation and found that material damping strengthens the overall filtering capability of 1-D periodic foundation. Meanwhile, the wave isolation capacity of 2-D and 3-D periodic foundations has also been studied extensively by a number of researchers [13–18].

In parallel to the research progress on the periodic foundation, the potential applications of periodic barriers have been investigated on both numerical and experimental fronts. For instance, Huang et al. [19] performed Finite Element Method (FEM) modeling to study the reduction characteristics of the periodic pile barrier subjected to plan waves and analyzed the effect of the pile parameters on the ground response behind the pile barrier. Pu et al. [20] conducted FEM to simulate the surface waves in a periodic pile and layered soil system and discussed the effect of multiple geometric parameters on the frequency band gaps and amplitude reduction spectrum. Pu et al. [21] also carried out a field experiment on periodic geofoam-filled trenches designed to block train-induced transient vibration. The results showed that screening effectiveness of the periodic barrier increases as the number of rows (unit cells) increases when the frequency of incoming surface wave falls into the frequency band gaps. Meng et al. [22] numerically studied the vibration mitigation capability of periodic pile barriers in saturated soil and under moving-load condition. The screening performance of the periodic barriers in other novel forms, including boreholes [23–25], cylindrical tubes [26,27], and rectangular prism containing a resonator [28], have also been assessed by researchers.

It can be noted that the aforementioned works are centered on wave isolation by either periodic barrier or periodic foundation. Few literatures have explored the potential of combining these two types of wave isolation structures. In fact, the frequency band gaps provided by the periodic barrier may differ from that of the periodic foundation due to: (1) the distinct geometric properties of the repeated unit cells, and (2) the different orientations of these buried structures when they are installed in place. Typically, the periodic foundation is placed horizontally beneath the superstructure while the periodic barrier is vertically inserted into the ground surface near the superstructure. As a result, different types of dominant waves propagate through the periodic foundation and periodic barrier when the system is subjected to excitation in a certain direction.

In October 2019, a field experiment was developed to assess the wave isolation performance of periodic barriers using NHERI@UTexas experimental facility at the Hornsby Bend site in Austin, Texas. This work has been presented by Huang et al. [29] with emphases on describing the field test procedure and evaluating the screening effectiveness of 1-D periodic barriers. In June 2020, a new field testing program incorporated with a 1-D periodic foundation and an enhanced ground motion sensor array was conducted. The scopes of the new testing program primarily include: (1) evaluating the wave isolation performance of the 1-D periodic foundation, and (2) exploring the feasibility of combining periodic foundation and periodic barrier as a passive wave isolation system to mitigate body wave and surface wave simultaneously. Numerous findings have been made by analyzing the data collected from the new testing program (dated June 2020) and by revisiting the data collected from the old testing program (dated October 2019).

This paper presents the field experiments dedicated to evaluating the screening effectiveness of a passive wave isolation system comprising both periodic barrier and periodic foundation to minimize the response of the protected superstructure. Under the excitation in a certain direction, the periodic foundation can serve as a complement to the periodic barrier by rejecting the energy outside the frequency band gap of the periodic barrier. Therefore, a wider frequency band gap can be obtained when periodic foundation and periodic barrier are combined to use. Furthermore, at frequency ranges where the frequency band gaps of periodic foundation and periodic barrier overlap, the filtering effects are added to each other, and the response of the superstructure is further reduced.

The field experiments presented in this study involve investigating the influence of exciting frequency and excitation directions on the screening effectiveness of a periodic barrier-foundation wave isoloation system. Both periodic barrier and periodic foundation are made of 1-D layered periodic material including reinforced concrete (RC) and polyurethane layers. The source of excitation is applied in three orthogonal directions (the vertical, horizontal crossline, and horizontal inline directions) separately using a state-of-art triaxial hydraulic mobile shaker. For each direction of excitation, three different forms of input signals (single-frequency, downward frequency-sweeping, and seismic excitations) that cover the frequency range of 15–100 Hz are adopted in the testing. Several barrier conditions are considered in this study, including the periodic barriers with various lengths and number of barriers. For comparison purposes, the empty trench is also included as one of the barrier conditions.

The remainder of the paper is organized as follows. Section 2 provides the details of (1) the experimental setup, (2) the methodology of conducting the field test for passive isolation test, and (3) data interpretation methods. In Section 3, the experimental test results are presented. The performance of periodic foundation and periodic barrier are discussed separately, which is followed by an evaluation of the overall screening effectiveness using the periodic barrier-periodic foundation system. Lastly, the conclusions are drawn in Section 4.

2. Experimental program

2.1. Test design and soil property

Depending on the location of the wave barriers, Woods [30] categorized the wave screening measures into active isolation and passive isolation. The passive isolation is defined as employment of barriers at a place close to the protected region/object to block the vibration from entering the protected region/object. The active isolation is defined as employment of barriers around the vibration source. In this study, the field tests can be classified as the passive isolation tests because the distance between the barrier and vibration source is maintained approximately five times as long as the distance between the barrier and protected object. The vibration source is generated by the hydraulic mobile shaker at a designated location. The protected object is a steel frame that has a dimension of 0.6 × 0.6 × 0.6 m.

The test site is part of the Hornsby Bend Biosolids Management Plant southeast of Austin, Texas. The Spectral-Analysis-of-Surface-Waves (SASW) testing conducted on the test site [29] shows that the topsoil layer located between 0 and 0.61 m below the ground surface has the shear wave velocity of 67.1 m/s, the second soil layer located between 0.6 and 2.1 m below the ground surface has the shear wave velocity of 161.5 m/s, and the soils between 2.1 and 5.8 m are considered as the third soil layer with the shear wave velocity of 234.7 m/s. The density measurement shows the soil at 0.3 m (1 ft) below the ground surface has a density of 1670 kg/m^3, and the density at 0.91 m (3 ft) below the ground surface is 1702 kg/m^3. The Poisson ratio is assumed to be 0.33 for unsaturated soils. Based on these results, Young's modulus is calculated as 20 MPa, 118 MPa, and 249 MPa in the first, second, and third layers, respectively.

Fig. 1 shows the schematic diagram of the various passive isolation systems (section view and plan view) and associated nomenclature used in this study. As shown in Fig. 1, the testing program includes the influence of barrier conditions discriminated by the infilled materials, the geometric arrangements, the number of barriers, and the foundation types. The natural-soil condition without any barriers or empty trench is first investigated to serves as a benchmark case (denoted as "S0"). The case with a 2.55 m-long empty trench is denoted as "EL". The case with a 1.22 m-long periodic barrier is denoted as "B1" (one unit cell of periodic material). The case with two parallel 1.22 m-long periodic barriers is denoted as "B2" (two unit cells of periodic material) and the case with a 2.44 m-long barrier is denoted as "BL" (a longer barrier with one unit cell of periodic material). Discriminated by the type of foundation used to support the steel frame, the usage of RC foundation and the usage of the periodic foundation are referred to as scenario P1 and scenario P2, respectively. Scenario P1 was reported by Huang et al. [29], while scenario P2 and the comparison between scenario P1 and scenario P2 are reported in this study. During the testing, the shaker is used to apply excitation on the ground surface on the left of the isolation systems shown in Fig. 1. Therefore, the waves generated by the shaker are deemed to propagate from left to right in the soils in these schematics.

The design procedure for the periodic barrier and periodic foundation involves determining theoretical frequency band gap based on the dispersion relationship of the 1-D periodic metamaterial given certain material properties and geometry of the constituents [29]. The theoretical frequency band gap derivations for P and S waves are described in detail by Witarto et al. [31] and the theoretical frequency band gap derivation for Rayleigh wave is presented by Huang [32]. The metamaterials (including RC and polyurethane) of the periodic barrier were optimized to maximize the theoretical frequency band gaps within the operating frequency range of the shaker (15–100 Hz). The selected periodic barrier has one unit cell comprising three layers of constituents. The first and third layers are RC layers with the following properties: $E_{RC} = 30.44$ GPa, $\rho_{RC} = 2400$ kg/m^3, $a_{RC} = 0.2$, $h_1 = 101.6$ mm. The second layer is polyurethane layers with the following properties: $E_{poly} = 0.1586$ MPa, $\rho_{poly} = 1100$ kg/m^3, $\nu_{poly} = 0.463$, $h_2 = 76.2$ mm.

Previous studies show that the more unit cells are present in the periodic material, the greater response reduction inside the frequency band gaps can be provided. Nonetheless, the frequency band gaps do not change with the increasing number of unit cells [33]. In order to widen the frequency band gaps, two unit cells with different compositions (i.e., having different frequency band gaps) can be combined to form a single unit cell. Thus, the one-unit cell periodic foundation used in this study is designed as a combination of two unit cells with different compositions. The selected periodic foundation is composed of three layers of 101.6 mm thick RC, and the two layers of 127 mm and 76.2 mm thick polyurethane. The RC layers and polyurethane layers are alternatively arranged.

The theoretical frequency band gaps within the range from 0 to 100 Hz for the periodic foundation and periodic barrier used in this study are listed in Table 1. As shown in Table 1, the dominant type of wave propagating through the periodic material is dependent on the excitation direction, which serves as a key factor in evaluating the performance of both periodic barrier and periodic foundation. The periodic barrier is designed to filter the waves propagating horizontally through the barrier. As a result, Rayleigh wave, S wave, and P wave are the major types of the wave filtered by the barrier when the excitation is applied in the vertical, horizontal crossline, and horizontal inline directions, respectively. On the other hand, the periodic foundation is designed to filter the waves propagating upward through the foundation. Therefore, P-wave and S-wave are the major types of waves filtered by the foundation when excitation is applied vertically and horizontally, respectively.

The different configurations of the wave barriers used in this study are listed in Table 2. One short periodic barrier (barrier condition B1) installed beneath the ground surface during the field testing is shown in Fig. 2. Since the study is intended to evaluate the performance of the periodic material that is buried in the soil, the bottom of the periodic foundation is also placed below the ground surface. The installation of the periodic foundation is shown in Fig. 3.

2.2. Test facility and excitation type

Fig. 4 shows the typical test setup for passive isolation tests. As

Table 1
Theoretical frequency band gaps of periodic barrier and periodic foundation.

Specimen	Excitation direction	Dominant wave type	Theoretical frequency band gaps
Periodic barrier	Horizontal inline	P wave	45.0–100 Hz
	Horizontal crossline	S wave	11.8–46.1, 49.1–92.1, and 93.7–100 Hz
	Vertical	Rayleigh wave	10.2–43.8, 47.0–87.6, and 88.8–100 Hz.
Periodic foundation	Vertical	P wave	32–39.7 and 54.9–100 Hz
	Horizontal inline and crossline	S wave	8.4–10.4, 14.4–48.5, and 49.2–100 Hz.

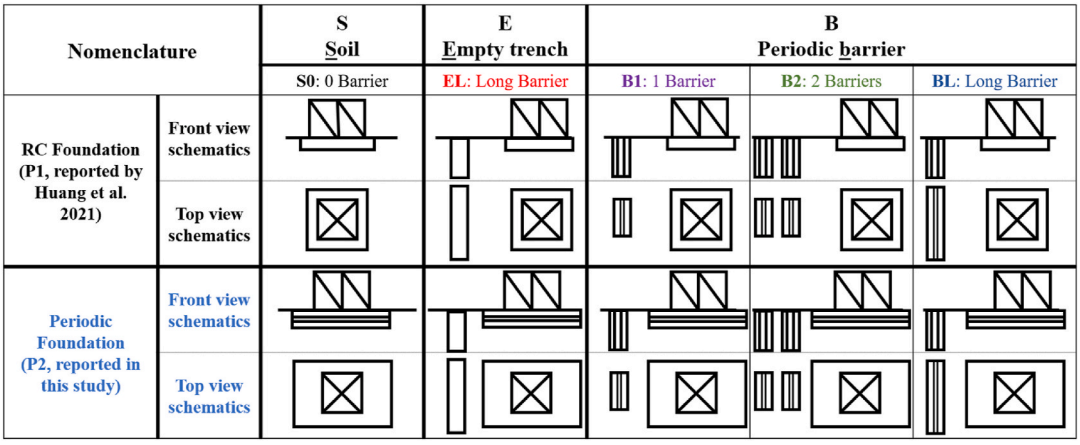

Fig. 1. Schematic showing testing configurations (not to scale) and nomenclature used in this study; the source of dynamic excitation is on the left of the isolation system.
Note: Scenario P1 was reported by Huang et al. [29], while scenario P2 and the comparison between scenario P1 and scenario P2 are discussed in this study. The tests in scenario P1 were completed in October 2019, while the tests in scenario P2 were completed in June 2020.

Table 2
Barrier dimensions.

Barrier condition	Description	Length (m)	Depth (m)	Width (m)
EL	One long empty trench	2.44	1.52	0.28
B1	One short periodic barrier	1.22	1.52	0.28
B2	Two periodic barriers separated by 2.62 m	1.22	1.52	0.28
BL	One long periodic barrier	2.44	1.52	0.28

Note: "Depth" represents the vertical dimension of the barrier, "Length" represents the longer horizontal dimension that is perpendicular to the wave propagation direction, and "Width" represents the shorter horizontal dimension that is along the wave-propagation direction.

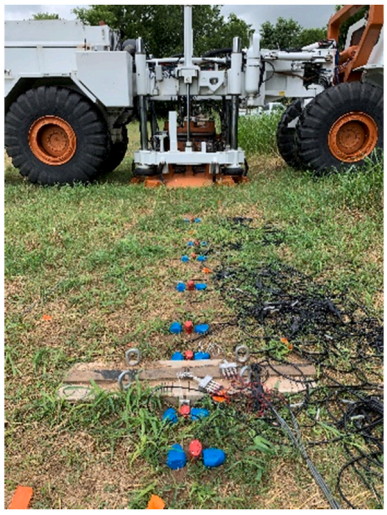

Fig. 2. Installed barrier and mobile shaker truck.

Fig. 3. Installation of periodic foundation.

shown in Fig. 4, the state-of-the-art hydraulic mobile shaker, named T-Rex, is used to generate the vibration on the ground surface at the designated location approximately 6 m (20 ft) away from the designated barrier location. Dynamic loading by T-Rex is applied separately in the three orthogonal (i.e., vertical, horizontal crossline, and horizontal inline) directions. In each direction, the vibration is supplied by three different types of excitation input signals, including 1) single-frequency cyclic excitations, 2) downward frequency-sweeping excitations (or chirp), and 3) seismic excitations using seismograms from real earthquake events [29]. Fig. 5 shows these three typical signals in the time domain and frequency domain. As shown in Fig. 5(a), the single-frequency cyclic excitations have a dominant output at 65 Hz in

Fig. 4. Typical passive isolation test setup.

the frequency domain. As shown in Fig. 5(b), the downward frequency-sweeping excitation has a relatively stable output at frequencies ranging from 15 Hz to 100 Hz. The seismic excitation based on the El Centro earthquake in time domain and frequency domain are shown in Fig. 5(c) and (d), respectively. The T-Rex shaker can stably generate the requested vibration without distorting the main frequency content of the signals.

2.3. Test measurement and frequency response function

Fig. 6 shows the arrangement of the geophones installed to measure the particle velocity of ground surface in the P2EL, P2BL, P2B1, and P2B2 series. The 3-D velocity response of the surface soil is collected by an array of 15 geophone stations, which are numbered as 1 through 15 in Fig. 6. Each geophone station consists of three 1-D geophones that are oriented in the three orthogonal directions. As shown in Fig. 6(b), for the P2B1 series, two 3-D accelerometers are installed at the left side (denoted as 5A) and right side (denoted as 6A) of the periodic barrier to further investigate the vibration isolation performance of periodic barrier itself. In addition, three 3-D accelerometers are attached to the top and bottom of the periodic foundation and the top of the steel frame to record the 3-D acceleration during the vibration events. The horizontal inline direction is along the geophone array and the horizontal crossline direction is perpendicular to the geophone array.

In this study, the Frequency Response Function (FRF) is used to quantify the screening effectiveness of the wave isolation system. The values of FRF are calculated using "average method" and "direct method" as defined in Appendix A. The average method accounts for multiple measuring points behind the wave barrier so it is used to evaluate the global screening effectiveness of the wave barriers. On the other hand, the direct method allows for evaluating the screening effectiveness of the wave barrier itself, excluding the energy dissipation associated with spatial damping and soil damping.

3. Experimental results

3.1. Screening effectiveness of the periodic foundation

3.1.1. FRF of the periodic foundation

During the passive isolation tests, the wave is assumed to propagate from the bottom to the top of the periodic foundation. By placing 3-D accelerometers on the path of wave transmission at the bottom and top of the periodic foundation, the filtering characteristic of the periodic foundation can be observed. Fig. 7(a), (c) and (e) show the response on

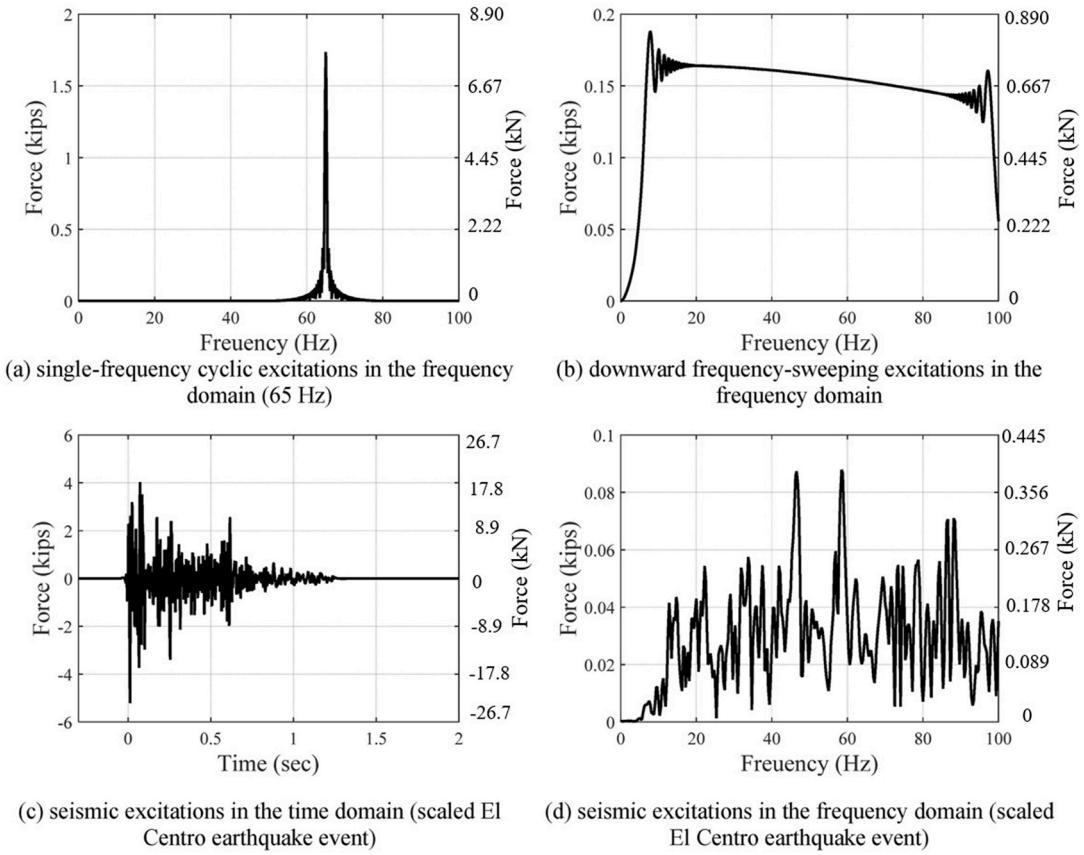

(a) single-frequency cyclic excitations in the frequency domain (65 Hz)

(b) downward frequency-sweeping excitations in the frequency domain

(c) seismic excitations in the time domain (scaled El Centro earthquake event)

(d) seismic excitations in the frequency domain (scaled El Centro earthquake event)

Fig. 5. Typical input driving signals for the shaker to generate vibration (Note: 1 kips equals 4.448 kN).

the top and bottom of the periodic foundation in the time domain when the downward frequency-sweeping excitation is applied in the vertical, horizontal crossline, and horizontal inline directions, respectively. Fig. 7 (b), (d) and (f) show the response of these two points in the frequency domain under the three directions of excitation, respectively. The response at these two points is collected during the same loading event. Therefore, the responses can be directly compared without the need for normalization. In Fig. 7 (b), the theoretical frequency band gaps of periodic foundation with respect to P wave are shaded with yellow color; in Fig. 7 (d) and (f), the theoretical frequency band gaps of periodic foundation with respect to S wave are shaded with yellow color. As shown in Fig. 7, the responses in different directions are different from each other. Overall, a significant reduction can be observed when the response at the top of the periodic foundation is compared with the response at the bottom of the periodic foundation. Some amplification is noted within 25–30 Hz when vertical excitation is applied.

Using the direct method, the response at the bottom of the periodic foundation is taken as $|A(f)|_{\text{enter}}$ and the response on the top of the periodic foundation is taken as $|A(f)|_{\text{exit}}$ in Eq. (A.3). Fig. 8 shows the resulting *FRF*s for excitation applied in all three directions. In Fig. 8(a), the theoretical frequency band gaps of periodic foundation subjected to P wave are shaded with yellow color; in Fig. 8(b) and (c), the theoretical frequency band gaps of periodic foundation subjected to S wave are shaded with yellow color. Each figure contains the results obtained from the excitation in all three forms. The attenuation zone determined from the field testing can be identified when the *FRF* is below zero. For each excitation direction, different forms of input signals render similar attenuation zones, which also show agreement with the theoretical frequency band gap as designed. When the periodic foundation is subjected to the vertical excitation (Fig. 8(a)), slight response amplification occurs below 35 Hz which is outside the frequency band gap for the P wave. As for Fig. 8(b) and (c), the attenuation zones occur within the entire 15–100 Hz when the horizontal crossline and horizontal inline excitations are applied, which are generally in line with the theoretical frequency band gaps of the S wave.

3.1.2. *Comparison of steel frame response with and without periodic foundation*

An alternative way to assess the screening effectiveness of the periodic foundation is to compare the response of the superstructure (the steel frame) when it is installed on RC foundation (scenario P1) and a periodic foundation (scenario P2). The responses on the top and bottom of the 10 cm-thick RC foundation are almost identical and any response modification caused by the RC foundation is negligible as compared to the periodic foundation. Therefore, scenario P1 can be used to represent the case without using the periodic foundation.

At each exciting frequency, the response of the steel frame is represented by the amplitude of steady-state acceleration time history measured by the accelerometer attached to the top of the steel frame. To compare the response of the steel frame between scenarios P1 and P2, the responses need to be normalized because the force output of the shaker may be varying even with identical input driving signals. The response is normalized by dividing the maximum steady-state response at top of the steel frame by the maximum steady-state response at the reference point, which is measured by the accelerometer attached to the bottom of the foundation.

The normalized response at the structure top for the cases with and without the periodic foundation is compared in Fig. 9. The data obtained under the single-frequency cyclic excitations in the vertical, horizontal crossline, or horizontal inline directions are shown in Fig. 9 (a), (b) and (c), respectively. For the cases without the periodic foundation, only the case P1S0 is presented; for the cases with the periodic foundation, only the case P2S0 is presented. Even though the responses are recorded for all test setups, the findings are fairly consistent regardless of whether a

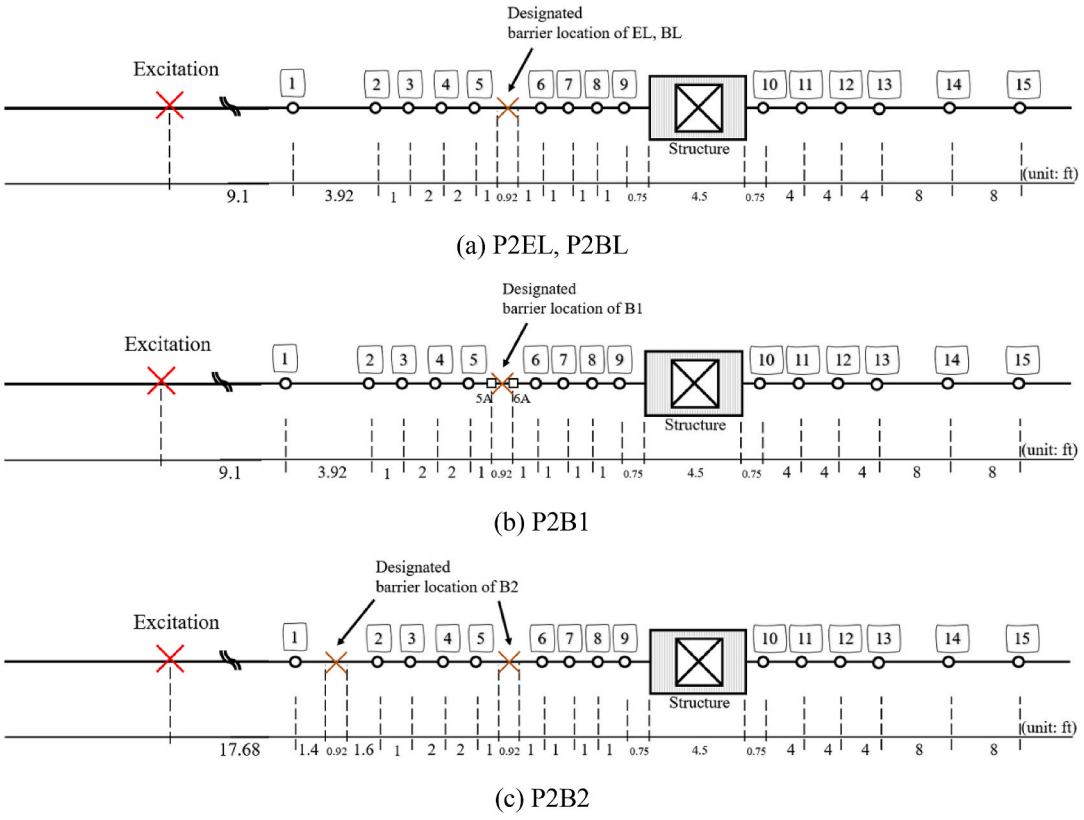

Fig. 6. Deployment of geophones for P2EL, P2BL, P2B1, and P2B2 series (not to scale, unit: ft, 1ft equals 0.305 m).
Note: Each of the geophone stations numbered from 1 to 15 consists of three 1-D geophones oriented orthogonally. 5A and 6A in Fig. 6(b) denote the locations where two 3D accelerometers are installed on the left and right sides of the periodic barrier, respectively.

barrier is used. Therefore, only cases P1S0 and P2S0 are used to demonstrate the effect of the periodic foundation on the structure response. Additionally, the selection of S0 can exclude the influence of the barrier so that only the effect of the periodic foundation is investigated.

As shown in Fig. 9, much less structure response is seen when the structure is placed on a periodic foundation than it would be when the structure is placed on a RC foundation. For the majority of the investigated frequency range (15 to 100 Hz), the structure response in all three directions of excitation can be greatly reduced by using the periodic foundation. As shown in Fig. 9(a) and (b), minor response amplification occurs for the frequencies below 30 Hz when the excitation is applied in the vertical and horizontal crossline directions.

3.2. Screening effectiveness of the wave barriers

3.2.1. FRF calculated using the direct method

The theoretical dispersion relation of the periodic barrier only considers the well-controlled materials, namely the RC and polyurethane layers. To entirely exclude the contribution of the soil layer to the performance of the barrier, only the response of the closest points on the two sides of the periodic barriers are taken into account when calculating the *FRF* for scenario B1. These two sensor locations are denoted as Point No.5A and Point No.6A in Fig. 10.

In Section 3.2, the screening effectiveness of the wave barrier is represented in the figure that has normalized depth (the corresponding exciting frequency is shown in the bracket) in the x-axis and *FRF* in the y-axis. The normalized depth is defined as the ratio of the physical depth of the barrier to the wavelength of the Rayleigh wave propagating in the first soil layer and is considered a key factor affecting the screening performance of the wave barrier. All the barriers used in this study have a physical depth of 1.52 m. The wavelength of the Rayleigh wave is calculated using the soil density and test results of the S wave velocity of the first soil layer. Attenuation zones are the ranges of frequency/normalized depth with negative *FRF*.

Fig. 11 shows the FRF of scenario B1 under single-frequency cyclic excitation evaluated using the direct method. The performance is found to be distinctive when the barrier is subjected to excitation in different directions. Rayleigh wave, S wave, and P wave are the dominant wave types filtered by the periodic barrier when the excitation is in the vertical, horizontal crossline, and horizontal inline directions, respectively. In Fig. 11, the theoretical frequency band gaps of the periodic barrier subjected to Rayleigh wave, S wave, and P wave are shaded with yellow color in Fig. 11 (a), (b), and (c), respectively. The results presented in Fig. 11 are obtained by the response collected by the accelerometers directly attached on the edge of the first and the last layer of the short periodic barrier (B1). It is observed that the attenuation zones identified via the field testing using the direct method coincide fairly well with the theoretical frequency band gaps for all the three exciting directions in Fig. 11(a), (b), and (c). Besides the response reduction located within the theoretical frequency band gap, Fig. 11(c) also shows the response amplification (FRF greater than zero) within the theoretical passband.

When it comes to combining the periodic foundation and periodic barrier in wave isolation systems, one concern is that the existence of periodic foundations might adversely affect the ground response behind the periodic barrier. Some of the energy that is not permitted to pass through the periodic foundation might be reflected to the earth. Consequently, the ground response near the periodic foundation might be amplified. This potential unfavorable effect caused by the periodic foundation can be investigated by comparing the FRF of the periodic barrier with the existence of the concrete foundation and that with the existence of the periodic foundation.

In Fig. 11, the FRF of the periodic barrier in the scenario P2 (with periodic foundation) is plotted together with the results of the scenario

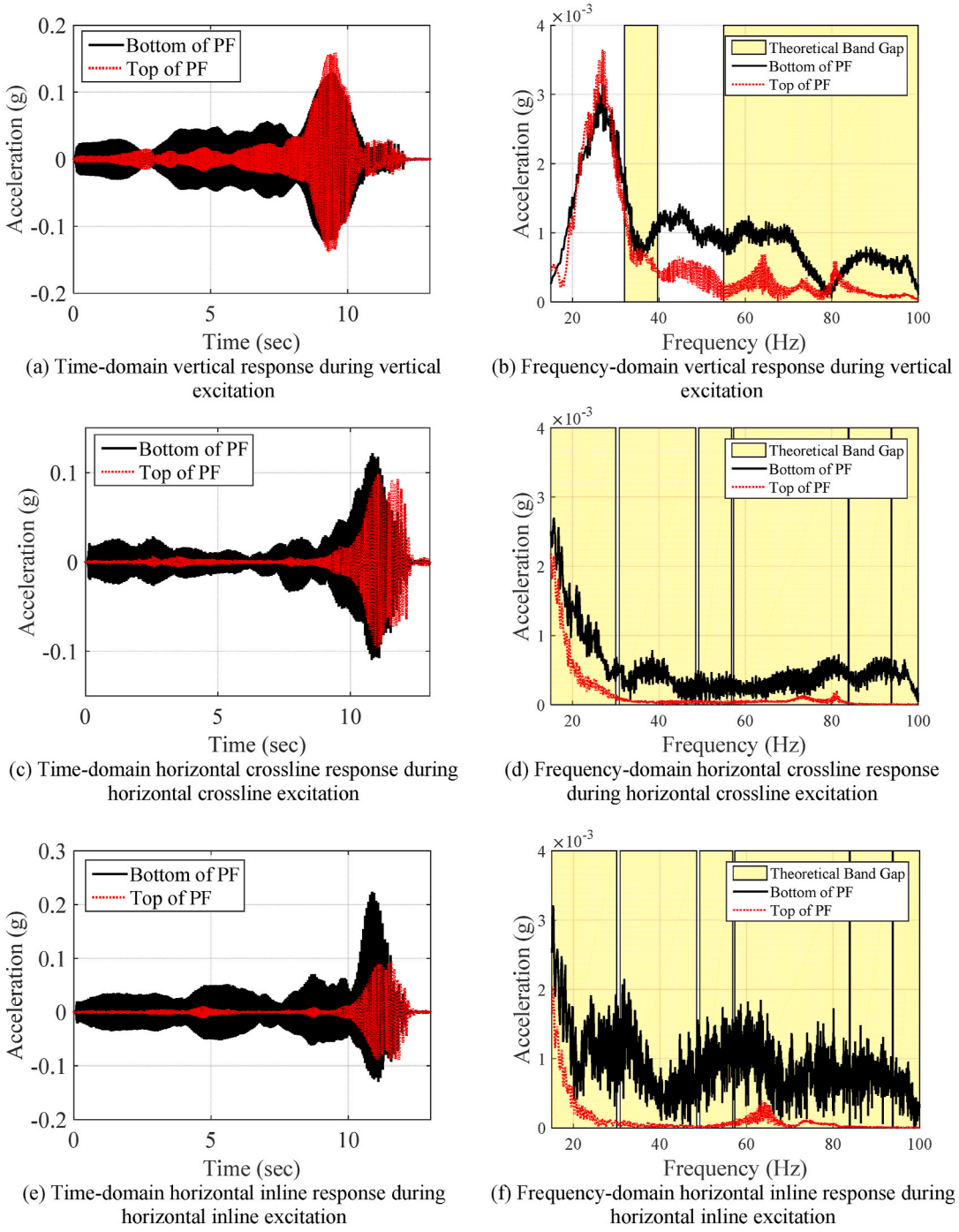

(a) Time-domain vertical response during vertical excitation

(b) Frequency-domain vertical response during vertical excitation

(c) Time-domain horizontal crossline response during horizontal crossline excitation

(d) Frequency-domain horizontal crossline response during horizontal crossline excitation

(e) Time-domain horizontal inline response during horizontal inline excitation

(f) Frequency-domain horizontal inline response during horizontal inline excitation

Fig. 7. Comparison of the acceleration response at the top and bottom of the periodic foundation (PF stands for periodic foundation).

P1 (with RC foundation). The *FRF* results of cases P1B1 and P2B1 are showing a certain level of similarity especially when the barrier is subjected to vertical excitation (Fig. 11(a)). For barriers subjected to horizontal excitation (Fig. 11(b) and (c)), although the *FRF* values of cases P1B1 and P2B1 exhibit some discrepancy, the attenuation zones are quite similar. For all three directions of excitation, the *FRF* results from the direct method indicate that the usage of the RC foundation or periodic foundation does not make a significant difference in the filtering ability of the periodic barrier.

3.2.2. *FRF calculated using the average method*

Using the average method with a measuring extent of 2.44 m, the FRF of vertical soil response during vertical excitation is presented in Fig. 12. By comparing across Fig. 12(a), (b), and (c), the results obtained from different types of input signals are found to be consistent, implying that the field test is well controlled and reliable. Moreover, since the data is processed differently for a different type of input signal, having the results in agreement with each other indicates that the calculation method is also reliable. As reported in previous research, the response reduction caused by the wave barriers is more significant when the normalized depth is greater than 0.6 [34–39]. In this study, the response amplification is observed for two short barriers (P2B2) and one long barrier (P2BL) even when the normalized depth is less than one. In the lower frequency range (i.e., below 40 Hz), the performance of all barrier conditions meet the expectations as follows: 1) the ground surface response is reduced after the barrier is installed; 2) the empty trench

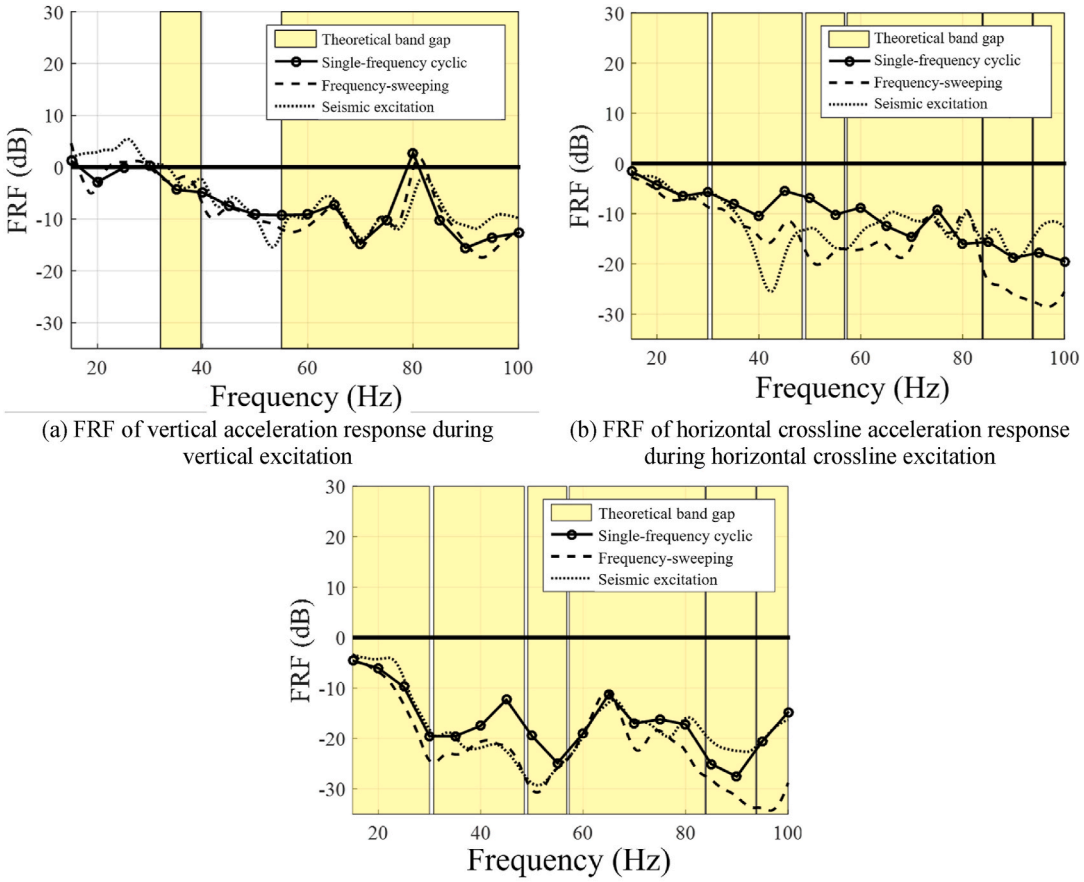

(a) FRF of vertical acceleration response during vertical excitation

(b) FRF of horizontal crossline acceleration response during horizontal crossline excitation

(c) FRF of horizontal inline acceleration response during horizontal inline excitation

Fig. 8. FRF of response at the periodic foundation in the benchmark case (P2S0); *FRF* is calculated by the direct method comparing the response between the top and the bottom of the periodic foundation.

(P2EL) outperforms the periodic barrier (P2BL) that has the same dimension; 3) the barrier with longer length has better screening effectiveness when comparing cases P2B1 and P2BL; 4) adding the second barrier improves the performance of the isolation system when comparing cases P2B1 with P2B2. The response amplification is observed for all barrier conditions at frequencies ranging from 45 Hz to 65 Hz even though the normalized depth is greater than one. Moreover, although the empty trench is expected to outperform all other barrier conditions for the exciting frequency greater than 70 Hz, the screening effectiveness of case P2EL is not as good as case P2B1.

Using the average method with a measuring extent of 2.44 m, the FRF of horizontal soil response during horizontal crossline and horizontal inline frequency-sweeping excitation are presented in Fig. 13(a) and (b), respectively. Comparison between the cases P2B1 and P2B2 in Fig. 13(a) shows that adding the second periodic barrier improves the overall screening effectiveness of the isolation system under the horizontal crossline excitation. In addition, the performance of a long empty trench P2EL appears to be less effective in reducing the ground surface response than a long periodic barrier P2BL, which further highlights the advantage of using periodic barriers in the wave isolation system. As shown in Fig. 13(b), when the excitation is applied in the horizontal inline direction, the single long empty trench P2EL displays the best screening effectiveness among all other barrier conditions, with the response reduction covering the entire frequency range of interest (15–100 Hz). In contrast to what is observed for case P2EL, the response amplification is observed for case P2B2 within the frequency range of 15 to 100 Hz. The wave isolation performance of one short barrier (P2B1) is notably better than two short periodic barriers (P2B2).

In order to investigate the potential amplification of the ground response caused by the periodic foundation as mentioned in Section 3.2.1, the average method is utilized to compare the screening effectiveness with the existence of the periodic foundation and that with the existence of RC foundation. In Table 3, the attenuation zones identified for the scenario P2 (with periodic foundation) are compared with the results of the scenario P1 (with RC foundation) reported from previous research [29]. The attenuation zones in both scenario P1 and scenario P2 are determined based on the ground surface response within the measuring extent of 2.44 m under different directions of excitation.

Comparison between scenarios P1 and P2 in Table 3 shows that the attenuation zones for all barrier conditions share a high level of similarity except for cases P1BL and P2BL. For barrier condition BL, the combination of the periodic foundation and long periodic barrier (P2BL) is favorable as it widens the attenuation zones when excitation is applied in horizontal crossline and horizontal inline directions. In case P2BL, the attenuation zones under both directions of horizontal excitation cover the entire frequency range of interest (15–100 Hz). However, for other periodic barrier conditions such as B1 and B2, the changes in ground response reduction induced by replacing the RC foundation with the periodic foundation are insignificant.

3.3. *Screening effectiveness of the periodic barrier-foundation system*

Based on the direct method, the FRF of combined periodic barrier-periodic foundation system can be defined as the superposition of the FRFs induced by the periodic barrier and periodic foundation, which is described by the following equations:

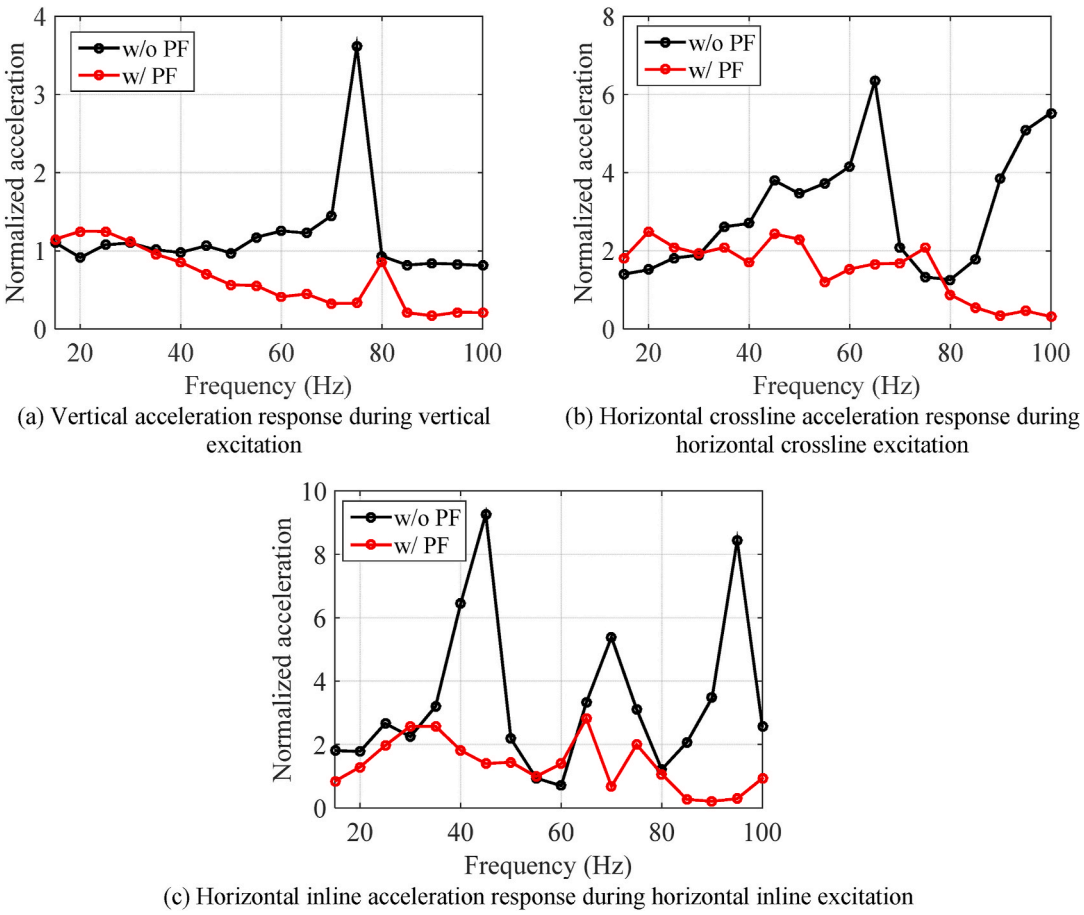

Fig. 9. Normalized acceleration response at the top of the steel frame w/and w/o the periodic foundation (PF stands for periodic foundation).

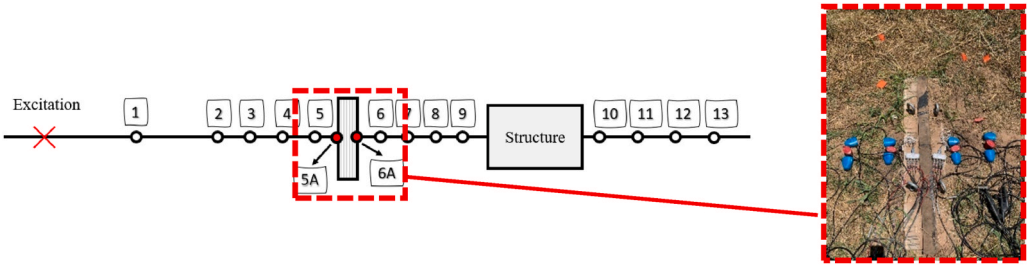

Fig. 10. Sensor layout utilized to evaluate the screening effectiveness of periodic barrier with the direct method in cases P1B1 and P2B1.

$$FRF\_\text{barrier}(f) = 20 \times \log_{10}\left[\left(\frac{|A(f)|_{\text{foundation\_bottom\_P2BL}}}{|A(f)|_{\text{Point5\_P2BL}}}\right) \Big/ \left(\frac{|A(f)|_{\text{foundation\_bottom\_P1S0}}}{|A(f)|_{\text{Point5\_P1S0}}}\right)\right] \tag{1}$$

$$FRF\_foundation(f) = 20 \times \log_{10}\left[\left(\frac{|A(f)|_{\text{foundation\_top\_P2BL}}}{|A(f)|_{\text{foundation\_bottom\_P2BL}}}\right) \Big/ \left(\frac{|A(f)|_{\text{foundation\_top\_P1S0}}}{|A(f)|_{\text{foundation\_bottom\_P1S0}}}\right)\right] \tag{2}$$

$$FRF\_all(f) = FRF\_barrier(f) + FRF\_foundation(f) \tag{3}$$

where $|A(f)|_{\text{foundation\_bottom\_P1S0}}$ denotes the normalized frequency-domain response at bottom of foundation for case P1S0 (with native soil and concrete foundation); $|A(f)|_{\text{point5\_P1S0}}$ denotes the normalized frequency-domain response at point No. 5 in soil (in front of the barrier as shown in Fig. 6) for case P1S0; $|A(f)|_{\text{foundation\_top\_P1S0}}$ denotes the normalized frequency-domain response on top of foundation for case P1S0. The subscript P2BL denotes the results obtained from case P2BL

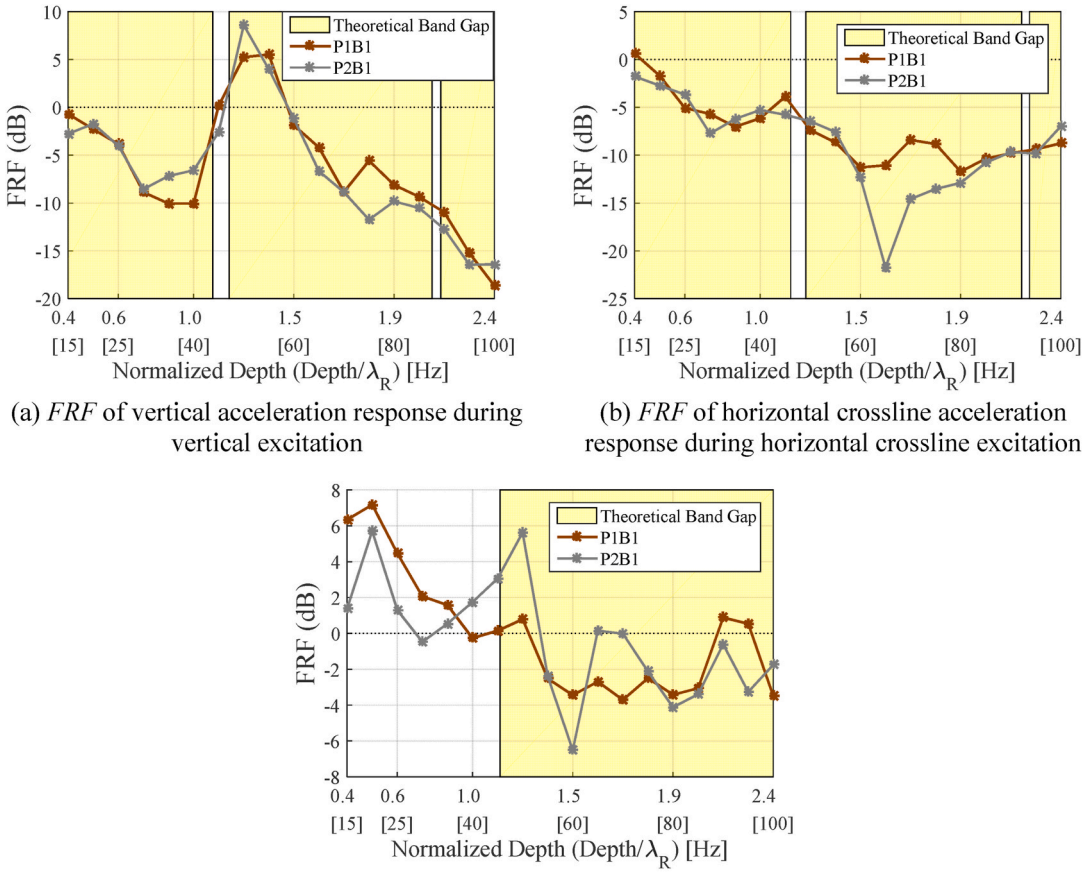

(a) *FRF* of vertical acceleration response during vertical excitation

(b) *FRF* of horizontal crossline acceleration response during horizontal crossline excitation

(c) *FRF* of horizontal inline acceleration response during horizontal inline excitation

Fig. 11. FRF of scenarios P1B1 and P2B1 under single-frequency cyclic excitation evaluated by the direct method (Enter: Point No.5A, Exit: Point No.6A).

(with the long periodic barrier and periodic foundation). *FRF_all* denotes the FRF of the system of long periodic barrier and periodic foundation. The purpose of dividing the responses in case P2BL by the corresponding responses in case P1S0 is to exclude the energy dissipation induced by spatial damping and soil damping in the calculation of *FRF_all*.

Fig. 14 compares the FRFs of the periodic barrier, periodic foundation, and combined system obtained from the average results of all seismic excitation tests. Fig. 14 shows that under the same direction of excitation, the FRF of the period barrier differs from the FRF of the periodic foundation over the frequencies of concern (15 to 100 Hz). The reason is that the periodic barrier and periodic foundation were not only constructed with different dimensions and arrangements of periodic materials but were also oriented perpendicularly to each other during the testing. The combined usage of periodic foundation and periodic barrier allows them to complement each other and provides a wider frequency band gap than either of them does.

Under the vertical excitation (Fig. 14(a)), slight response amplification of the system is observed at two low-frequency ranges ([15 Hz, 21 Hz] and [25 Hz, 38 Hz]), which is mostly attributed to the amplification associated with the periodic foundation. However, for vertical excitation at frequencies between 38 Hz and 100 Hz, significant attenuation is observed for the system of periodic barrier and periodic foundation.

As shown in both Fig. 14(b) and (c), the FRF of the periodic barrier-periodic foundation system stays low at the frequency ranging from 15 Hz to 100 Hz. In comparison, using either periodic barrier or periodic foundation alone cannot achieve consistent vibration mitigation with such low values of FRF at this frequency range. The results in Fig. 14 provide engineers with insights on the seismic isolation performance using both periodic foundation and periodic barrier, which will facilitate the design of these facilities in engineering practice to mitigate earthquake or vibration with a specific direction or frequency range. In this study, the mechanical performance of periodic barrier-foundation system is reported in detail. Deep-learning-based simulation [40] and finite element simulation [41] are recommended for future study to achieve high-accuracy prediction of the vibration isolation performance of periodic barrier-foundation system in both frequeny domain and time domain. In addition, nonlinear model updating algorithm [42] are recommended to obtain optimized finite element model for the test system and to guide engineering design and simulation of periodic barrier-foundation systems. Based on high-fidelity model of soil, periodic barriers, periodic foundations and structural system [43,44], the simulation accuracy of engineering structures with various barrier-foundation systems can be notably enhanced to achieve performance-based design of periodic barriers, periodic foundations and structural system.

4. Conclusions

This paper presents an experimental study to investigate the screening effectiveness of a passive wave isolation system consisting of both periodic barrier and periodic foundation. At a distance from the wave isolation system, dynamic loading is created by a mobile shaker truck and is applied in three orthogonal directions using three types of input signals. The screening effectiveness, quantified as FRF, of the periodic barrier, periodic foundation, and the entire periodic barrier - periodic foundation system is evaluated based on both direct method and average method. The conclusions drawn from this study are as follows:

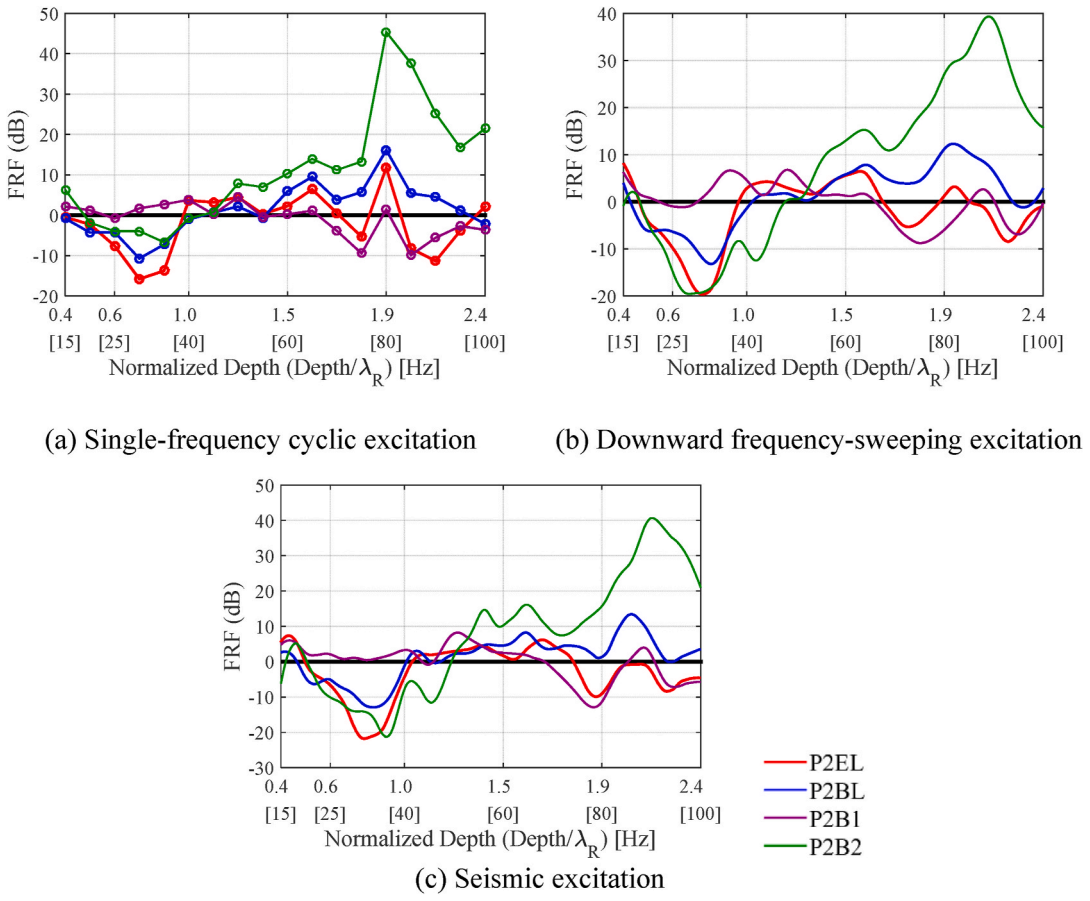

Fig. 12. FRF of vertical velocity response during vertical excitation evaluated by the average method with measuring extent of 2.44 m (red: P2EL, blue: P2BL, purple: P2B1, green: P2B2).

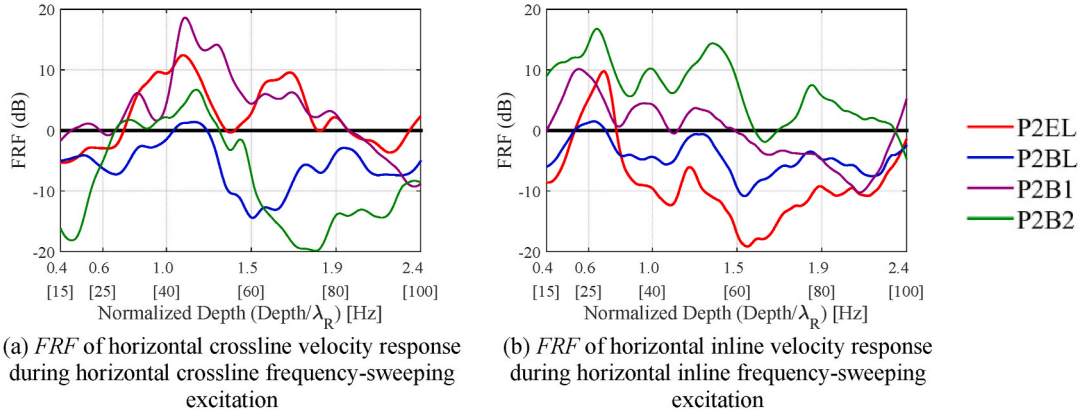

Fig. 13. FRF of horizontal velocity response during horizontal downward frequency-sweeping excitation evaluated by the average method with measuring extent of 2.44 m (red: P2EL, blue: P2BL, purple: P2B1, green: P2B2).

1. Different types of input signals used in the field tests lead to similar *FRF* results for the periodic barrier and periodic foundation, indicating the reliability of the field test results.
2. Excitation direction plays an important role in evaluating the screening performance of periodic foundation because different dominant waves transmit through the foundation when the protected object is subject to different directions of excitation. For the periodic foundation used in this study, the computed FRF under vertical excitation ranges from 3 to −17 dB while the computed FRF under horizontal excitation ranges from −1 to −34 dB at the operating frequency range of the shaker (15–100 Hz).
3. The attenuation zones derived from the direct method are compared with the theoretical frequency band gap with the assumption that only the dominant type of wave generated by the excitation in a certain direction is considered. For both periodic barrier and periodic foundation, the response reduction occurs within the frequency ranges that match the theoretical frequency band gaps.
4. When it comes to combining the periodic foundation and periodic barrier in wave isolation systems, one concern is that some energy that is not permitted to transmit through the periodic foundation might be reflected to the earth, amplifying the ground response behind the periodic barrier. This potentially unfavorable effect

Table 3
Attenuation zones of scenarios P1 and P2 from average method with measuring extent of 2.44 m

Loading direction	Barrier condition	P1: RC foundation		P2: Periodic foundation	
		Attenuation zone (Hz)	Maximum response reduction (%)	Attenuation zone (Hz)	Maximum response reduction (%)
Vertical	EL	20-40, 70-80	89	20-40, 70-100	90
	BL	20-40, 80-100	78	15–40	79
	B1	65–100	86	65–100	76
	B2	15–50	94	15–50	90
Horizontal crossline	EL	15-30, 65-100	67	15-30, 85-100	64
	BL	15-20, 90-100	81	15–100	88
	B1	15-30, 85-100	98	85–100	81
	B2	15–100	92	15-25, 60-100	92
Horizontal inline	EL	15-20, 35-100	93	15-20, 30-100	93
	BL	60-70, 75-100	77	15–100	82
	B1	60-70, 75-100	91	60–100	86
	B2	None	N/A	None	N/A

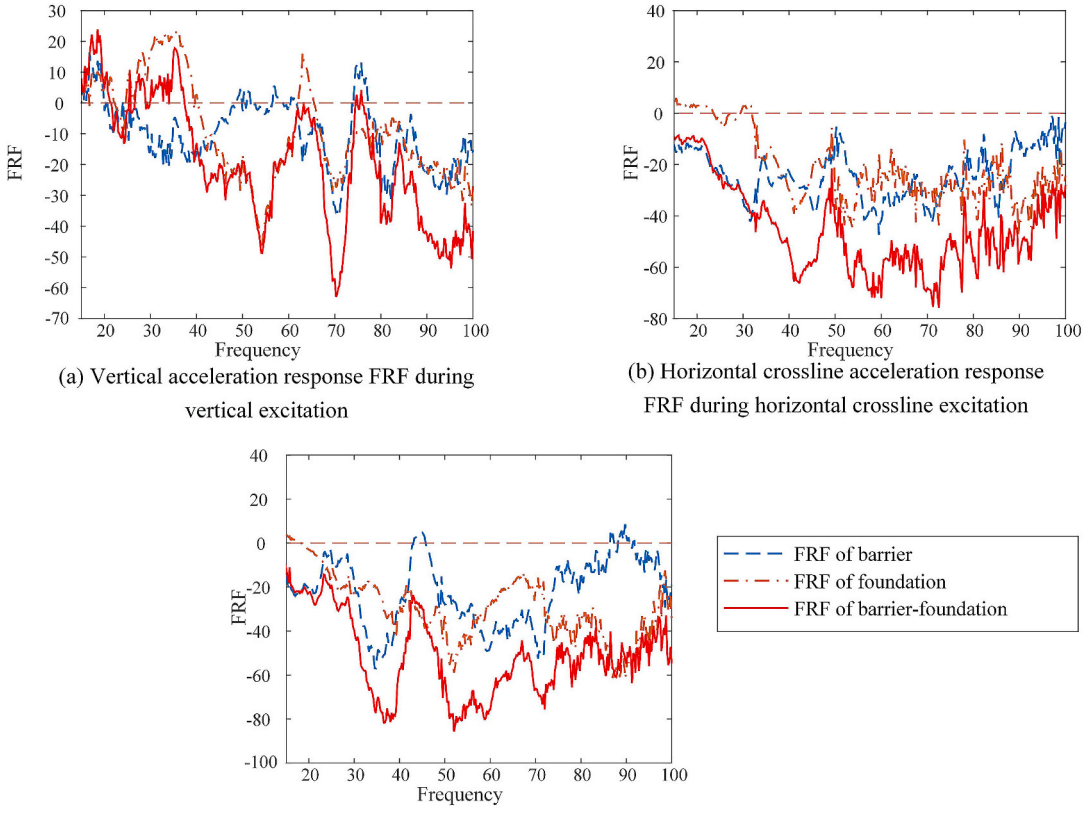

(a) Vertical acceleration response FRF during vertical excitation

(b) Horizontal crossline acceleration response FRF during horizontal crossline excitation

(c) Horizontal inline acceleration response FRF during horizontal inline excitation

Fig. 14. FRF of the wave isolation system composed of the periodic barrier and periodic foundation obtained from the average result of all seismic excitation tests.

caused by the periodic foundation can be investigated by comparing the FRF of the periodic barrier with the existence of the concrete foundation and that with the existence of the periodic foundation. In this study, no evidence is found that the existence of the periodic foundation could impact screening performance of the periodic barrier.

5. Given a certain direction of excitation, the dominant wave types affecting the periodic barrier and periodic foundation are different and, therefore, frequency band gaps induced by the periodic barrier and periodic foundation are different. The combined usage of the periodic barrier and the periodic foundation allows for response reduction of the superstructure over a frequency range wider than the frequency bang gap created by using either of them.

Author statement

Benchen Zhang: Field test, Investigation, Validation, Data Curation; **Hsuan Wen Huang**: Field test, Writing-Original Draft, Writing-Review & Editing; Methodology, Visualization; **Jiaji Wang**: Writing-Original Draft, Writing-Review & Editing, Methodology, Formal analysis, Visualization; **F. -Y. Menq**: Writing-Review & Editing, Field test, Data Curation, Resources; **Kalyana Babu Nakshatrala:** Writing-Review & Editing, Validation, Supervision; **Y. L. Mo:** Writing-Review & Editing, Resources, Supervision, Project administration, Funding acquisition; **K. H. Stokoe**: Writing-Review & Editing, Resources, Supervision, Project administration, Funding acquisition.

Data availability statement

All data, models, or code that support the findings of this study are available from the corresponding author upon reasonable request.

Declaration of competing interest

The authors declare that they have no known competing financial interests or personal relationships that could have appeared to influence the work reported in this paper.

Acknowledgments

The authors would like to express gratitude to the U.S. National Science Foundation for the financial support under grant 1761659. The authors are also thankful to the NHERI@UTexas team for their assistance in the field experiments.

Appendix A

In this study, two different approaches are used to calculate the *FRF* for various wave barriers: "average method" and "direct method". In the average method, the generalized response of several measuring points behind the wave barriers is compared with that of the same points in the benchmark case (S0). In the direct method, the response at the entering face of the periodic barrier or periodic foundation is compared with that at the exiting face. For both approaches, only the response in the same direction as the excitation is considered for evaluating the performance of the isolation system. The average method and direction method are described in detail as follows.

A.1. Average method

For the average method, the equation used to calculate FRF depends on the form of the input signal. In the cases of using single-frequency cyclic excitation, the dynamic signals measured by geophones usually start with outstanding spikes and then transition to steady-state cycling with stable amplitude. These spikes are removed from the time series before the amplitude of the steady-state cyclic response is determined for each measuring point. Using Eq. (A.1), FRF can be calculated for a certain exciting frequency.

$$\overline{FRF}_{f_i} = 20 \times \log_{10}\left(\frac{1}{L}\int_0^L \frac{\left|\widehat{A}_{w,f_i}(t)\right|_{\max}}{\left|\widehat{A}_{wo,f_i}(t)\right|_{\max}} dx\right) \tag{A.1}$$

where f_i is the exciting frequency of the single-frequency excitation, $\left|\widehat{A}_{wf_i}(t)\right|_{\max}$ is the normalized response of the ground surface in the cases with wave barriers installed, $\left|\widehat{A}_{wof_i}(t)\right|_{\max}$ is the normalized response in the benchmark case with no wave barrier (S0), and L is the measuring extent, which is the distance from the barrier to the farthest measuring point used in the average method.

In the cases of using frequency-sweeping excitation and seismic excitation, the response is transformed into the frequency domain by Fast Fourier Transform (FFT). Therefore, the calculated FRF is a continuous function of frequency as described in Eq. (A.2).

$$\overline{FRF}\left(f\right) = 20 \times \log_{10}\left(\frac{1}{L}\int_0^L \frac{\left|\widehat{A}_w(f)\right|}{\left|\widehat{A}_{wo}(f)\right|} dx\right) \tag{A.2}$$

where $|\widehat{A}_w(f)|$ is the normalized frequency-domain response in the scenarios with wave barriers installed, $|\widehat{A}_{wo}(f)|$ is the normalized frequency-domain response in the benchmark scenario with no wave barrier (S0). For seismic excitation, nine seismograms from different historical earthquake events are utilized as the input signals to drive the shaker. The reported *FRF* in this study represents the average level of *FRF* obtained from all nine earthquake events.

One challenge of the average method lies in that the actual force output of the shaker may vary from event to event even when the shaker is supplied with identical input signals. In order to eliminate the impact of inconsistent output performance of the hydraulic vibration source, the soil response needs to be normalized to compare various barrier scenarios with the benchmark case (S0). This normalization is achieved by dividing the response of a measuring point by the response at the reference point, which is selected as the closest point to the side of the barrier facing the vibration source. By comparing the normalized ground surface response between the various barrier scenarios and the benchmark scenario (S0), the *FRF* can be calculated.

A.2. Direct method

The direct method evaluates the performance of the periodic material by comparing the response at entering face and exiting face of the periodic material. The response at entering face of the periodic material is denoted as $|A(f)|_{\text{enter}}$ and the response at the exiting face of the periodic material is denoted as $|A(f)|_{\text{exit}}$. Therefore, the FRF in the direct method can be expressed as follows:

$$FRF(f) = 20 \times \log_{10}\left(\frac{|A(f)|_{\text{exit}}}{|A(f)|_{\text{enter}}}\right) \tag{A.3}$$

The response at entering face and exiting face of the periodic barrier are collected by the sensors located at the front and back edges of the barrier. The response at entering face and exiting face of the periodic foundation is collected by the sensors located at the top and bottom of the periodic foundation. The direct method allows for comparing the response on the two sides of the wave barrier without any normalization effort that is needed in the average method.

References

[1] Huang J, Shi Z, Huang W, Chen X, Zhang Z. A periodic foundation with rotational oscillators for extremely low-frequency seismic isolation: analysis and experimental verification. Smart Mater Struct 2017;26(3):035061.
[2] Xiang HJ, Shi ZF, Wang SJ, Mo YL. Periodic materials-based vibration attenuation in layered foundations: experimental validation. Smart Mater Struct 2012;21(11):112003.
[3] Witarto W, Wang SJ, Yang CY, Wang Jiaji, Mo YL, Chang KC, et al. Three-dimensional periodic materials as seismic base isolator for nuclear infrastructure. AIP Adv 2019;9(4):045014.
[4] Yan Y, Laskar A, Cheng Z, Menq F, Tang Y, Mo YL, Shi Z. Seismic isolation of two dimensional periodic foundations. J Appl Phys 2014;116(4):044908.
[5] Yan Y, Cheng Z, Menq F, Mo YL, Tang Y, Shi Z. Three dimensional periodic foundations for base seismic isolation. Smart Mater Struct 2015;24(7):075006.
[6] Pu X, Shi Z. Periodic pile barriers for Rayleigh wave isolation in a poroelastic half-space. Soil Dynam Earthq Eng 2019;121:75–86.
[7] Pu X, Shi Z. Broadband surface wave attenuation in periodic trench barriers. J Sound Vib 2020;468:115130.
[8] Bao J, Shi Z, Xiang H. Dynamic responses of a structure with periodic foundations. J Eng Mech 2012;138(7):761–9.
[9] Xiang HJ, Shi ZF, Wang SJ, Mo YL. Periodic materials-based vibration attenuation in layered foundations: experimental validation. Smart Mater Struct 2012;21(11):112003.
[10] Zhao C, Zeng C, Huang H, Dai J, Bai W, Wang J, Mo YL. Preliminary study on the periodic base isolation effectiveness and experimental validation. Eng Struct 2021;226:111364.
[11] Shi Z, Cheng Z, Xiang H. Seismic isolation foundations with effective attenuation zones. Soil Dynam Earthq Eng 2014;57:143–51.
[12] Cheng Z, Shi Z, Palermo A, Xiang H, Guo W, Marzani A. Seismic vibrations attenuation via damped layered periodic foundations. Eng Struct 2020;211:110427.
[13] Cheng ZB, Shi ZF. Composite periodic foundation and its application for seismic isolation. Earthq Eng Struct Dynam 2018;47(4):925–44.
[14] Cheng Z, Shi Z. Novel composite periodic structures with attenuation zones. Eng Struct 2013;56:1271–82.
[15] Yan Y, Laskar A, Cheng Z, Menq F, Tang Y, Mo YL, Shi Z. Seismic isolation of two dimensional periodic foundations. J Appl Phys 2014;116(4):044908.
[16] Yan Y, Cheng Z, Menq F, Mo YL, Tang Y, Shi Z. Three dimensional periodic foundations for base seismic isolation. Smart Mater Struct 2015;24(7):075006.
[17] Shi Z, Huang J. Feasibility of reducing three-dimensional wave energy by introducing periodic foundations. Soil Dynam Earthq Eng 2013;50:204–12.
[18] Cheng Z, Yan YQ, Menq FY, Mo YL, Xiang HJ, Shi ZF, Stokoe KH. 3D periodic foundation-based structural vibration isolation. In: Proceedings of the world congress on engineering, vol. 3; 2013, July. p. 1797–802.
[19] Huang J, Shi Z. Attenuation zones of periodic pile barriers and its application in vibration reduction for plane waves. J Sound Vib 2013;332(19):4423–39.
[20] Pu X, Shi Z. Surface-wave attenuation by periodic pile barriers in layered soils. Construct Build Mater 2018;180:177–87.
[21] Pu X, Shi Z, Xiang H. Feasibility of ambient vibration screening by periodic geofoam-filled trenches. Soil Dynam Earthq Eng 2018;104:228–35.
[22] Meng L, Cheng Z, Shi Z. Vibration mitigation in saturated soil by periodic pile barriers. Comput Geotech 2020;117:103251.
[23] Meseguer F, Holgado M, Caballero D, Benaches N, Sanchez-Dehesa J, López C, Llinares J. Rayleigh-wave attenuation by a semi-infinite two-dimensional elastic-band-gap crystal. Phys Rev B 1999;59(19):12169.
[24] Brûlé S, Javelaud EH, Enoch S, Guenneau S. Experiments on seismic metamaterials: molding surface waves. Phys Rev Lett 2014;112(13):133901.
[25] Brûlé S, Enoch S, Guenneau S. Experimental evidence of auxetic features in seismic metamaterials: ellipticity of seismic Rayleigh waves for subsurface architectured ground with holes. arXiv preprint; 2018. arXiv:1809.05841.
[26] Krödel S, Thomé N, Daraio C. Wide band-gap seismic metastructures. Extreme Mechanics Letters 2015;4:111–7.
[27] Palermo A, Krödel S, Marzani A, Daraio C. Engineered metabarrier as shield from seismic surface waves. Sci Rep 2016;6(1):1–10.
[28] Zeng Y, Peng P, Du QJ, Wang YS. A novel zero-frequency seismic metamaterial. 2019. arXiv preprint arXiv:1907.06446.
[29] Huang HW, Zhang B, Wang Jiaji, Menq FY, Nakshatrala KB, Mo YL, et al. Experimental study on wave isolation performance of periodic barriers. Soil Dynam Earthq Eng 2021;144:106602.
[30] Woods RD. Screening of surface wave in soils. J Soil Mech Found Div 1968;94(4):951–79.
[31] Witarto Witarto, Wang SJ, Yang CY, Nie Xin, Mo YL, Chang KC, Tang Yu, Kassawara Robert. Robert Kassawara. Seismic isolation of small modular reactors using metamaterials. AIP Adv 2018;8(4). 045307.
[32] Huang HW. Periodic metamaterial-based seismic isolation barriers: field studies and computational modeling (Doctoral dissertation). Department of Civil and Environmental Engineering, University of Houston; 2020.
[33] Witarto W. Periodic material-based seismic base isolators for small modular reactors (Doctoral dissertation). Department of Civil and Environmental Engineering, University of Houston; 2018.
[34] Al-Hussaini TM, Ahmad S. Design of wave barriers for reduction of horizontal ground vibration. J. Geotech. Eng. 1991;117(4):616–36.
[35] Alzawi A, El Naggar MH. Full scale experimental study on vibration scattering using open and in-filled (GeoFoam) wave barriers. Soil Dynam Earthq Eng 2011;31(3):306–17.
[36] Coulier P, Cuéllar V, Degrande G, Lombaert G. Experimental and numerical evaluation of the effectiveness of a stiff wave barrier in the soil. Soil Dynam Earthq Eng 2015;77:238–53.
[37] Persson P, Persson K, Sandberg G. Numerical study of reduction in ground vibrations by using barriers. Eng Struct 2016;115:18–27.
[38] Thompson DJ, Jiang J, Toward MGR, Hussein MFM, Ntotsios E, Dijckmans A, Degrande G. Reducing railway-induced ground-borne vibration by using open trenches and soft-filled barriers. Soil Dynam Earthq Eng 2016;88:45–59.
[39] Saikia A. Numerical study on screening of surface waves using a pair of softer backfilled trenches. Soil Dynam Earthq Eng 2014;65:206–13.
[40] Wang Jia-Ji, Wang Chen, Fan Jian-Sheng, Mo YL. A deep learning framework for constitutive modeling based on temporal convolutional network. Journal of Computational Physics 2022;449:110784.
[41] Huang Hsuan Wen, Wang Jiaji, Zhao Chunfeng, Mo YL. Two-dimensional finite-element simulation of periodic barriers. Journal of Engineering Mechanics 2021;147(2).
[42] Wang Jia-Ji, Liu Cheng, Nie Xin, Fan Jian-Sheng, Zhu Ying-Jie. Nonlinear model updating algorithm for biaxial reinforced concrete constitutive models of shear walls. Journal of Building Engineering 2021;44:103215.
[43] Wang Jia-Ji, Liu Cheng, Fan Jian-Sheng, Jerome HajjarF. Triaxial concrete constitutive model for simulation of composite plate shear wall–concrete encased: THUC3. Journal of Structural Engineering 2019;145(9).
[44] Wang Jia-Ji, Liu Cheng, Nie Xin, Ding Ran. Biaxial constitutive models for simulation of low-aspect-ratio reinforced concrete shear walls. Journal of Engineering Mechanics 2022;148(2).